DOI: 10.13009/EUCASS2023-438
Aerospace Europe Conference 2023 – 10TH EUCASS – 9TH CEAS

Investigation of a Cathode-Vapour-Feed Electrolyser for a Water Electrolysis Propulsion System

Sören Heizmann[⋆†], *Armin Herbertz*[⋆⋆], *Juliusz Saryczew*[⋆⋆] *and Chiara Manfletti*[⋆]
[⋆]*Technical University of Munich (TUM)*
85221 Ottobrunn, Germany
[⋆⋆]European Space Agency (ESA)
2201 AZ Noordwijk, Netherlands
s.heizmann@tum.de · armin.herbertz@esa.int · juliusz.saryczew@esa.int · chiara.manfletti@tum.de
[†]Corresponding author

Abstract

PEM-electrolysers using the Cathode-Vapour-Feed (CVF) concept are currently considered to show the most promising capabilities for use within a Water Electrolysis Propulsion (WEP) system. However, only very limited data about the concept's performance is publicly available so far. Therefore, such an electrolyser has been designed and tested at the European Space Agency (ESA) to identify any areas which require additional research. This paper describes the design of the developed electrolyser prototype and presents various test results, incl. polarization curves, transient behaviours during nominal operation as well as performance collapses at high temperatures.

1. Introduction

In recent years we have seen a significant change in the space industry as more satellites then ever before are being launched every year. It is predicted that 4.5 times more spacecraft will be sent to space by the end of this decade, causing various challenges [1]. The production cost per satellite will have to decrease in order to serve the growing demand and the increasing number of satellites will cause the necessity to perform collision avoidance manoeuvres more frequently. This also means that more spacecraft will require propulsion systems to enable safe operations and to ensure compliance with the European Code of Conduct for Space Debris Mitigation. As of now, most propulsion systems are using highly toxic propellants like hydrazine and its derivatives, causing the need to apply extensive safety measures when handling propulsion system components. This makes the development of new equipment as well as testing and integration of already existing equipment complex and therefore expensive. Even electric propulsion systems often rely on scarce gases like Xenon with a limited yearly production, giving the propellant cost a significant impact on the overall propulsion system cost. This circumstance and many other reasons are driving the continuous search for alternative solutions using green propellants.

One of the most promising green propulsion technologies is Water Electrolysis Propulsion (WEP) [2] [3]. In such a system the spacecraft is filled on ground with pure water instead of conventional and highly reactive propellants. Once in space an electrolyser is used to decompose the water into its components, hydrogen and oxygen. The generated gases can subsequently be stored in smaller intermediate tanks or directly be used in chemical or electrical thrusters to propel the spacecraft.

The technology is currently in development at several companies and universities in Europe, while the two key components are the respective thrusters and the electrolyser. So far only a few electrolysers have ever been flown to

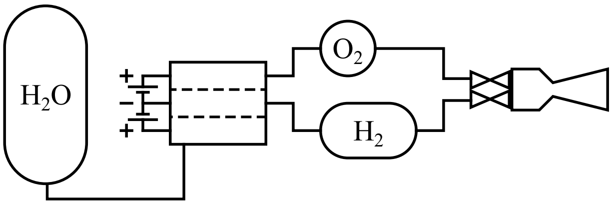

Figure 1: Concept of Water Electrolysis Propulsion using a Cathode-Vapour-Feed electrolyser

DOI: 10.13009/EUCASS2023-438

space. And although the demand for green hydrogen is causing the topic of water electrolysis to become a growing research field for terrestrial applications, the operation of an electrolyser in the space environment is causing many particular challenges. These are for example the separation of the process water from the generated gases, the choice of appropriate methods to pressurize them and to achieve gas qualities that are suitable for the utilized thrusters. The European Space Agency (ESA) has therefore decided to investigate the most promising electrolyser type for WEP. This shall create a better understanding of the component and shall help to identify areas which might require additional research and development to ensure a successful maturation of the technology towards flight readiness. The following paragraphs will describe the design of the electrolyser as well as its measured performance characteristics during several test campaigns.

2. Fundamentals of Electrolysis

The process of water electrolysis is a reduction-oxidation reaction, which is driven by the flow of electrical current. As the reaction is endothermic, energy in the form of direct current and heat has to be provided in order to split up the water molecule into its components. The required energy is equal to the standard enthalpy of formation ΔH_R^0, thus the reaction can be described by equation 1.

$$2\,\mathrm{H_2O_{(l)}} + \Delta\mathrm{H_R^0} \longrightarrow 2\,\mathrm{H_{2(g)}} + \mathrm{O_{2(g)}} \tag{1}$$

However, the complete reaction is composed of two half-reactions on each of the electrodes. During the decomposition of the water on the anode, the oxygen releases electrons (oxidation). While the created positively charged hydrogen ions (i.e. protons) receive electrons on the cathode (reduction). In water electrolysis the anode is therefore represented by the positive electrode and the cathode by the negative electrode.

Anode reaction:

$$2\,\mathrm{H_2O_{(l)}} \longrightarrow \mathrm{O_{2(g)}} + 4\,\mathrm{H^+} + 4\,\mathrm{e^-} \tag{2}$$

Cathode reaction:

$$4\,\mathrm{H^+} + 4\,\mathrm{e^-} \longrightarrow 2\,\mathrm{H_{2(g)}} \tag{3}$$

While the voltage provides the required energy to drive the reaction, the flowing current defines the hydrogen mass being produced. As commonly known, this is described by Faraday's laws of electrolysis (see equation 4). As the electrolysis reaction only occurs on the surfaces of the electrodes, it is common standard to divide the flowing current by the active area of the electrodes (A_{aa}) to receive the current density j. Using this approach differently sized electrolysers can be compared objectively regarding their performance.

$$m_{\mathrm{H_2}} = \frac{I\,t\,M_{\mathrm{H_2}}}{z\,F} \tag{4}$$

$$j = \frac{I}{A_{aa}} \tag{5}$$

In all experiments described in this paper, liquid water is decomposed and therefore the necessary energy for the reaction ΔH_R^0 is equal to the higher heating value of hydrogen (HHV). The minimum required voltage to enable the reaction without providing additional heat can therefore be calculated using equation 6 [4]. The resulting value is called the thermoneutral voltage U_{th}.

$$U_{th}^0 = \frac{\Delta H_R^0}{zF} = \frac{285.83\,\mathrm{kJ/mol}}{2 \times 96\,485.3\,\mathrm{C/mol}} = 1.481\,\mathrm{V} \tag{6}$$

However, there are also various losses which need to be overcome in order to let the reaction take place. One of the most significant losses is the ohmic loss U_{ohm}, which occurs due to the electrical resistance of the electrodes themselves and any electrical contact resistance between the different components. In addition, there are mass transport losses U_{mt} which become especially relevant for Cathode-Vapour-Feed electrolysers. As these losses are typically increasing with increasing current, the relation between the applied voltage and the current density is commonly shown in a respective chart, in which it forms a polarisation curve. In simple terms it can be said that the flatter and lower the curve is, the better the performance of the electrolyser is.

DOI: 10.13009/EUCASS2023-438

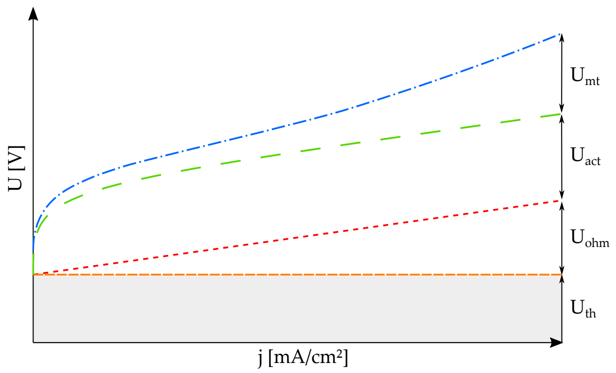

Figure 2: Qualitative composition of a polarisation curve of a PEM-electrolyser [4]

3. Cathode-Vapour-Feed Electrolyser

In the field of water electrolysis, Proton-Exchange-Membrane (PEM) electrolysers are becoming the most used technology to generate green hydrogen. The typical operation concept of such terrestrial electrolysers is the Liquid-Anode-Feed (LAF) (see figure 3). Here, the water is fed directly to the anode of the of the electrolyser, where it is decomposed into oxygen, protons (H^+) and electrons (see equation 2). Anode and cathode are separated by the thin Proton-Exchange-Membrane, which is designed to be only permeable for protons. The voltage applied on the electrodes creates an electrical potential that pulls the protons through the membrane to the cathode. The electrons move through the external circuit from the anode to the cathode, where they recombine with the protons to form hydrogen (see equation 3). Using this principle, the gases are already separated from each other during their production. In terrestrial applications the gases can raise as bubbles to the surface of the process water where they can be collected. One of the main advantages of the LAF technology is, that the gases can already be pressurized during their production. However, in a micro-gravity environment it causes significant challenges to separate the gases from the process water, as the density difference between the fluids can no longer be used to separate them.

To overcome this issue the concept can therefore be adapted to operate in Cathode-Vapour-Feed (CVF) (see figure 4). In this concept the water is fed to the cathode-side of the electrolysis membrane (ELYM) and an additional membrane between ELYM and the water is introduced, the so-called Water-Feed-Barrier (WFB). Within this principle the water has to diffuse through the WFB at first and is subsequently present in a vapour state inside the H_2-cavity. Afterwards, it diffuses through the ELYM as well, where it reaches the anode and is decomposed following the same principle as in LAF. The diffusion itself is caused by the concentration gradient of the water across the various layers of the electrolyser.

By diffusion the oxygen in the O_2-cavity can also migrate through the ELYM (see figure 5). However, the Pt catalyst on the cathode will cause it to recombine with the present H_2 to react to water again. Similarly, the hydrogen can migrate through the WFB to the water side where it might form bubbles, blocking off the water from moving

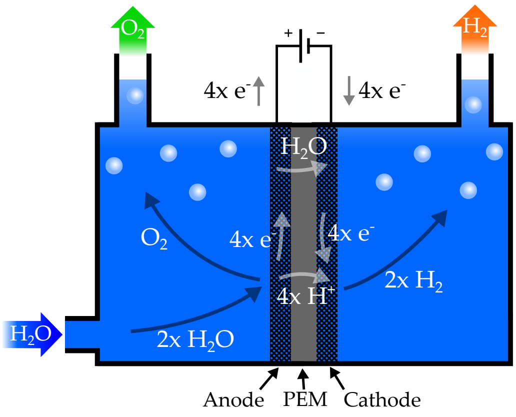

Figure 3: Concept of a Liquid-Anode-Feed (LAF) PEM electrolyser [5]

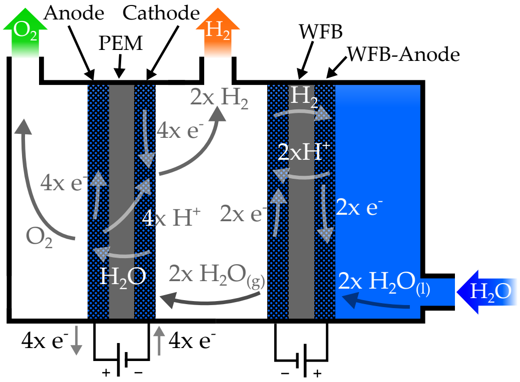

Figure 4: Concept of a Cathode-Vapour-Feed (CVF) PEM electrolyser [5]

DOI: 10.13009/EUCASS2023-438

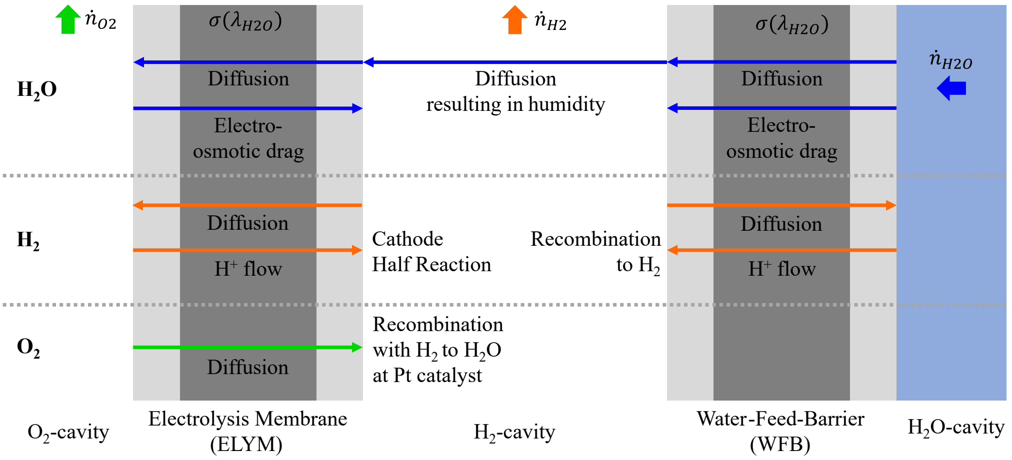

Figure 5: Summary of the various mass transport phenomena inside a CVF electrolyser

through the WFB towards the ELYM. To counteract this issue, a small voltage is applied onto the WFB effectively creating an electrochemical hydrogen pump. The voltage decomposes the hydrogen atoms into protons and electrons. Afterwards, the protons are pulled by the electric field to the other side of the membrane where they recombine with the electrons that moved through the external circuit. Subsequently, they recombine in the H_2-cavity again in the same way as on the ELYM. The required voltage for this process U_{Nernst} is defined by the Nernst-equation and is dependant on the temperature and pressure on either side of the WFB, as shown in equation 7 [4].

$$U_{Nernst} = \frac{\mathcal{R}\,T}{z\,F} ln\left(\frac{p^{cat}}{p^{an}}\right) \tag{7}$$

The higher the pressure difference between the H_2O- and H_2-cavity is, the more voltage has to be applied. However, even for a pressure ratio of 10 (i.e. $p^{an} = 10\,\text{bar}$ and $p^{cat} = 100\,\text{bar}$) and at a temperature of 70 °C this only results in a required voltage of 0.034 V. Hence, the power consumption is negligibly small compared to the one on the ELYM. In addition, there is also a positive side effect of the continuous pumping of hydrogen from the H_2O-cavity to the H_2-cavity. By electro-osmotic drag each proton moving through the membrane also drags a certain amount of water molecules with it to the other side of the WFB and therefore enhances the mass transport of the water towards the ELYM [6].

In addition, the proton conductivity of the membrane σ depends on its hydration level λ_{H_2O} [7]. The water also faces much more resistance until it reaches the anode-side of the ELYM compared to LAF. It is therefore of significant importance to improve the mass transport of the water through the cell as much as possible. Nevertheless, these factors cause a lower performance of the CVF concept compared to LAF. As the main advantage of a CVF electrolyser – the direct supply with liquid water free gases – is not important for terrestrial applications, there has subsequently been only very limited research and development work on the technology in Europe so far. Only a few CVF-electrolysers have ever been built in Europe and there are no information publicly available about its behaviour at the intended operating conditions for its utilization in a WEP system. It especially remains unclear how the water transport through the different layers of the electrolyser can be improved, as well as its behaviour at different temperatures and pressure levels. The presented work is therefore intending to close some of the current knowledge gap.

4. Electrolyser Design

The overall goal of the investigation was to gain a more detailed insight into the behaviour of a CVF electrolyser. Therefore, the focus of the design was enabling to test different configurations of the electrolyser. Hence, it was intended to achieve a simple assembly and disassembly process and that various components can be changed easily. Therefore, the compression bolts are not going through the monopolar plates as usual and the electrolyser is much heavier and bulkier then it could be expected from a flight-like design. Nevertheless, it has also been intended to significantly increase its performance in comparison to the proof-of-concept CVF electrolyser presented in [5] and [8]. In general, the design was based on a previous work of the corresponding author and incorporates several lessons learnt (see [5]). The electrolyser consists of a single cell with 3 monopolar plates realising the 3 cavities for O_2, H_2 and H_2O shown in figure 6 . The plates are made out of Titanium Grade 5 (Ti-6Al-4V) and each of them is equipped with a lug to connect the power supply cables and secure them via bolts. Each monopolar plate also features a simple flow field

DOI: 10.13009/EUCASS2023-438

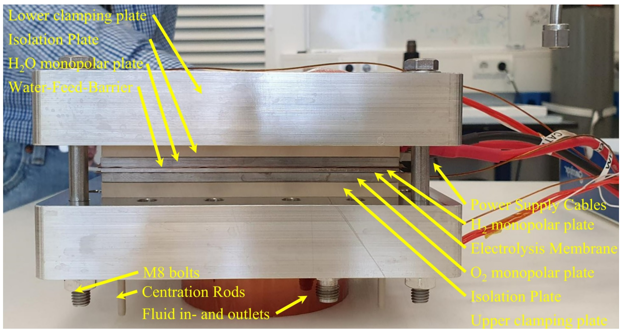

Figure 6: Electrolyser during its assembly

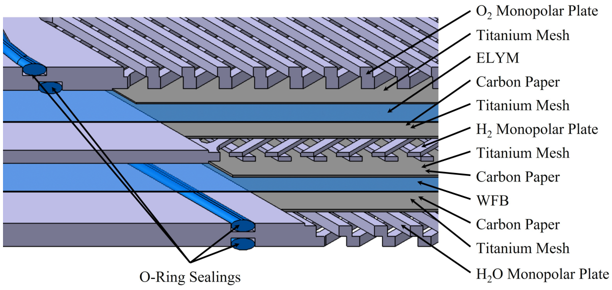

Figure 7: Internal design of the electrolyser showing its 3 dimensional flow field

as shown in figure 7, enabling the fluids to flow in all three spatial dimensions. The flow field itself has a dimension of 71 mm × 71 mm and has therefore the same shape and size as the active area A_{aa} of the membranes (i.e. catalyst coated area). The electrolyser therefore has an active area of 50.4 cm^2. In order to quantify the blockage caused by the flow field for the water diffusion, its porosity can be calculated as the ratio between its open and closed area. This results in a porosity of the flow field of 64.4%.

$$\Phi_{flowfield} = \frac{A_{open}}{A_{aa}} = \frac{32.46\,\text{cm}^2}{50.4\,\text{cm}^2} = 64.4\% \tag{8}$$

In addition, the monopolar plates feature a pocket to accommodate the Current Collectors (CC) and Gas Diffusion Layers (GDL) to create a flush surface with respect to the outer part of the monopolar plate (see figure 7). Therefore, the distance between the electrolysis membrane (ELYM) and the Water-Feed-Barrier (WFB) is defined by the H_2-monopolar plate, which has a thickness of 2 mm. For some test configurations additional Kapton© or Mylar© foils were glued to the H_2-monopolar plate to compensate manufacturing tolerances. The distance between the membranes scales accordingly. As current collectors, platinized titanium meshes with a thickness of 0.2 mm to 0.3 mm were used and for the GDLs carbon paper from Freudenberg was utilized. For the ELYM and the WFB a catalyst coated membrane (CCM) was employed. The CCM consisted of a Nafion© N115 membrane, which was coated with 1.0 mg/cm^2 Pt on the cathode side and with 2.0 mg/cm^2 Ir on the anode side. The catalyst coated area had the same shape and size as the flow field and therefore had an active area of 50.4 cm^2. With this size a sufficiently large gas production rate for potential volume flow measurements could be ensured, while keeping the requirements for the necessary power supply as low as possible. The 3 monopolar plates were isolated from the clamping plates via 2 isolation plates made out of PEEK. The whole stack was sealed using EPDM O-rings to achieve a good sealing inside the electrolyser and was compressed by two 30 mm thick clamping plates made of 1.4404 stainless steel. The relatively thick dimension of the plates was chosen in order to have a very stiff structure to achieve good sealing capabilities. Up to 20 M8 bolts can be used to compress the complete stack. However, initial commissioning tests showed repeated issues with membrane punctures caused by the high applied compression and the fibres at the edges of the titanium mesh. Therefore, only 4 bolts were used during all presented test campaigns. However, as all tests were conducted at atmospheric pressures no leakage issues became apparent. The in and outlet channels of the fluids are leading perpendicular to the membranes through the stack and are connected via 1/8” NPT-threads.

The electrolyser is equipped with one 75 W heater on the top clamping plate and a 100 W heater on the bottom clamping plate in order to enable a quick heat-up to the desired testing temperature. This is necessary as the two clamping plates exhibit a relatively high heat capacity. Both heaters are actively controlled via a simple on-off principle. The temperatures at the top and bottom clamping plate are compared with the desired temperature setpoint with a frequency

Parameter	**Value**
Outer Dimensions	175 mm × 175 mm × 100 mm
Total Mass	~16.5 kg
Stack Mass	~700 g
Max. power consumption	38.5 W
Voltage range	up to 2 V
Current range	up to 19.25 A

Parameter	**Value**
Pressure range	up to 100 bar
Temperature range	up to 80 °C
Membranes	Nafion© N115
Active Area	50.4 cm^2
Catalyst anode	2.0 mg/cm^2 Ir
Catalyst cathode	1.0 mg/cm^2 Pt

Table 1: Main electrolyser specifications

DOI: 10.13009/EUCASS2023-438

of 5 Hz and are switched on or off when falling below or exceeding the setpoint. Therefore, the electrolyser is equipped with one Type K thermocouple on each of the outer sides of the clamping plates and an additional thermocouple is applied on the outer surface of the H_2-monopolar plate to measure the temperature of the electrolysers centre. The main specifications of the electrolyser are summarized in table 1.

5. Test Bench

During the development of the electrolyser a Water Electrolysis Propulsion test bench was developed to facilitate electrolyser testing and performance evaluation. The test bench is located in the ESA Propulsion Laboratory at the European Space Research and Technology Centre (ESTEC). The development process and design justification for the WEP test bench is presented in more detail in another publication [9].

The WEP test bench was developed and assembled in-house. It was designed as a portable platform to allow for easy transportation and flexible interfacing with other facilities, such as vacuum chambers. The WEP test bench comprises a flow rig consisting of three fluidic branches for the water supply, as well as for oxygen and hydrogen discharge, respectively. Each branch has been equipped with fluidic components and measurement instrumentation to monitor and record the properties of the fluids, such as pressure, temperature and hydrogen concentration. The branches are mounted on a vertical plate, which provides convenient access to all components, including hand valves, and allows for clear tracing of fluid flow paths for process analysing. The branches are connected to the electrolyser, which is placed on a horizontal plate within an polystyrene enclosure for thermal insulation. The insulation enclosure prevents heat convection from the electrolyser, ensuring a stable thermal environment throughout the electrolyser testing process. It also allows to assume that the dissipated heat by the electrolyser is equal to 0, simplifying the evaluation of test results.

The WEP test bench has been undergoing continuous development, with its equipment being adjusted according to the specific test objectives. The design of the test rig is therefore not consolidated, and is evolving in line with the electrolyser testing process. At the time of the conducted test campaigns, parameters such as gas temperature and pressure were being measured in both branches of the test rig. Moreover, the hydrogen branch is equipped with a binary gas analyser to measure the hydrogen concentration, providing valuable information on the cross-diffusion across the membranes. In a later stage it has also been intended to combine it with a mass flow meter to determine the faradaic efficiency of the electrolyser.

Each of the water, oxygen and hydrogen branches have been equipped with a pressure transducer and a Type K thermocouple to accurately measure the fluid parameters. The water branch includes a 1-litre double-ended water tank. In the current test configuration, water is supplied to the electrolyser gravitationally, however the test bench allows for interfacing with a pressurant to test at increased water supply pressures. The tank is refilled through the top inlet. All components of the test rig are rated for pressures up to 70 bar. Additionally, each branch is equipped with a burst disk which acts as a safety measure against potential over-pressurization. The burst pressure of the burst disks falls within a range of 40-50 bar. To control the operation pressure of hydrogen and oxygen in the electrolyser the test bench is further equipped with back-pressure regulators on each branch theoretically allowing operation pressures of up to 100 bar.

The second platform of the WEP test bench is dedicated to the Data Acquisition system (DAQ) and the required

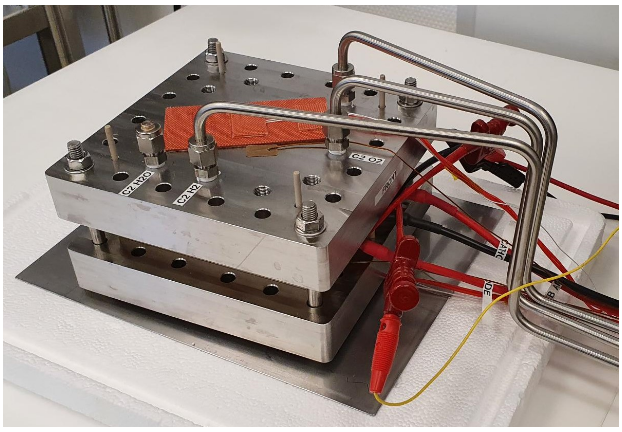

Figure 8: Electrolyser connected to the test bench with alligator clips used to measure the applied voltage directly at the monopolar plates

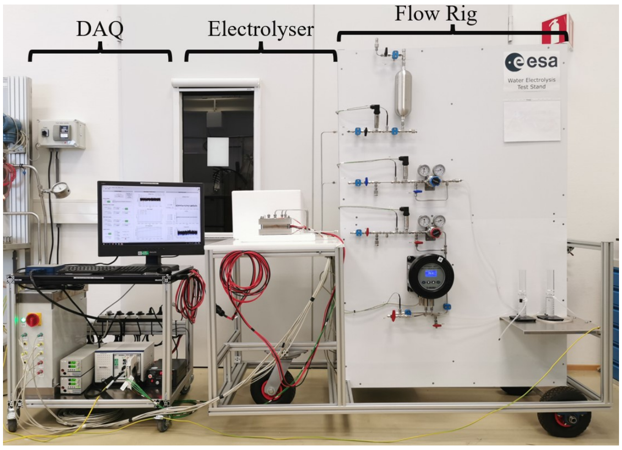

Figure 9: Configuration of the test bench during the presented test campaigns

power supplies. The DAQ platform has been split up from the WEP test bench to separate the operator from the area where potential presence of combustible gas may occur due to unintended leakage. Measurement data, commands, and power supply between the DAQ system and WEP test bench are transmitted by leads. The DAQ platform computer has been procured from National Instruments, and runs an in-house developed LabView program to control the WEP test bench. The DAQ has been equipped with a monitor to display the parameters of the electrolyser in a graphical user interface (GUI). The DAQ also commands the TDK Lambda Z^+10-40 power supplies which are used to operate the electrolyser. The power supplies are able to provide a voltage of up to 10 V and up to 40 A.

The WEP test bench serves not only for electrolyser characterisation and performance evaluation, but also for supporting end-to-end tests with thrusters. A test campaign with the first end-to-end coupling of an electrolyser and a Hall Effect Thruster has been performed in the ESA Propulsion Laboratory in 2023 [10].

6. Test Results and Evaluation

6.1 Test set-up and Testing Operations

Following the first assembly of the electrolyser various commissioning tests were performed, leading to several minor adaptations of the DAQ, the electrolyser and its components. Afterwards, the electrolyser could be successfully operated and a total of three test campaigns were conducted. Each consisting of multiple test runs to determine the electrolyser's polarisation curve at a specific temperature. While each test campaign represents a minor adjustment of the electrolyser's configuration.

During test campaign 1 (TC1), carbon paper of type H14CX485 from Freudenberg was used as Gas Diffusion Layer (GDL) on all membrane sides, except for the O_2-side of the electrolysis membrane (ELYM). This carbon paper type is equipped with a microporous layer, which shall enhance the mass transport of the fluids passing through the Membrane Electrode Assembly (MEA). To further improve the even distribution of current across the active area of the membrane, a platinized titanium mesh with a thickness of 0.2 mm-0.3 mm was utilized as current collector (CC) between the carbon paper and the monopolar plates, as well as directly on the O_2-side of the ELYM. In addition, the H_2 monopolar plate was equipped with a 51 µm thick Mylar© gasket on the ELYM-side and a 165 µm thick Kapton© gasket on the WFB-side. The purpose of these gaskets were both to serve as additional sealing aide between the different layers of the electrolyser and to compensate manufacturing inaccuracies of the pocket depth which is foreseen for the GDLs and CCs. Due to the large uncertainty of the thickness of the platinized titanium mesh, the compression of the GDLs could not be determined sufficiently well. Hence in the worst case, the configuration exhibited an insufficient contact between the monopolar plates and the membranes. However, the distance between the membranes can be assumed as 2.2 mm.

In an attempt to further improve the performance of the electrolyser, it has been tried to improve the contact between the monopolar plates and the CCs by changing the configuration of the gaskets. Therefore, the electrolyser was

Table 2: Electrolyser set-up for the different test campaigns

Layer	**TC 1**	**TC2**	**TC3**
CVF O_2 monopolar plate			
ELYM-GDL on O_2 side	Ti mesh	Ti mesh	Ti mesh
Electrolysis membrane (ELYM)	Nafion© N115 CCM	Nafion© N115 CCM	Nafion© N115 CCM
ELYM-GDL on H_2 side	H14CX483 + Ti mesh	H14CX483 + Ti mesh	H15C14 + Ti mesh
Gasket on ELYM side	51 µmMylar©	none	none
CVF H_2 monopolar plate			
Gasket on WFB side	165 µm Kapton©	165 µm Kapton©	165 µmKapton© + 51 µmMylar©
WFB-GDL on H_2 side	H14CX483 + Ti mesh	H14CX483 + Ti mesh	H15C14 + Ti mesh
Water Feed Barrier (WFB)	Nafion© N115 CCM	Nafion© N115 CCM	Nafion© N115 CCM
WFB-GDL on H_2O side	H14CX483 + Ti mesh	H14CX483 + Ti mesh	H14CX483 + Ti mesh
CVF H_2O monopolar plate			
Operating Temperatures	30, 2×40, 2×50, 2×60, 2×70, 75, 3×80 °C	40, 50, 60, 70 °C	40, 2×50, 2×60, 2×70, 80 °C

DOI: 10.13009/EUCASS2023-438

Table 3: Specifications of the carbon paper from Freudenberg used for the Gas Diffusion Layers [11]

	H14 CX 483	**H15C14**
Thickness at 0.025 MPa	180 µm	190 µm
Thickness at 1 MPa	142 µm	150 µm
Compressibility	21.1%	21.1%
Microporous Layer	Yes	Yes

disassembled and thoroughly cleaned. Afterwards, it was re-assembled using only one 165 µm thick Kapton© gasket on the ELYM-side of the H_2 monopolar plate. This resulted only in a minor change of the membrane distance. During the assembly, the membranes and GDLs of test campaign 1 were re-used. However, in the subsequently conducted second test campaign (TC2) a performance decrease of up to 46 mA/cm^2 could be observed. It was assumed that the most probable cause for this behaviour has been a partial delamination or another damage of the catalyst layer of the catalyst coated membrane (CCM), as well as a damage of the GDL's micro porous layer during the disassembly and re-assembly process.

In order to restore the electrolysers performance to its original state it was decided to replace the CCMs and GDLs with new ones. Due to supply issues the previous H14CX485 material for the GDL could not be re-used. Therefore, the very similar H15C14 material from the same manufacturer was utilized, which features a MPL as well. Using this set-up of the electrolyser a third test campaign (TC3) was conducted.

During all test runs of the different test campaigns the supply voltage of the electrolyser was set at the power supply. Each of these voltage settings provided by the power supply will be further referred as set point. Hence, the electrolyser was always drawing as much current as possible and was therefore operated in a voltage controlled operation mode. While the current was measured by the power supply, the applied voltage at the electrolyser was measured directly at the monopolar plates. The long power cables that were necessary due to the spatial conditions of the test bench, led to noticeable voltage drops between the power supply and the monopolar plates. This voltage drop can also be seen in the graphs that are shown in the following. The measurement of the applied voltage to the electrolyser at the monopolar plates was therefore particularly important, as only via this method credible measurements could be acquired. For the WFB, a voltage of 0.4 V was set at the power supply. As all tests were conducted at atmospheric pressure this allowed a sufficient margin beyond the required Nernst-voltage. Hence, it could be ensured that all hydrogen that might have diffused through the WFB could be pumped back to the H_2-cavity of the H_2 monopolar plate.

The heaters on the electrolyser were mostly used for a relatively quick heat up to the desired testing temperature, as well as to maintain constant temperature conditions during the test runs. During the test runs all parameters were measured and controlled with a frequency of 5 Hz. Throughout the test campaigns, various samples of the used distilled water were tested for their electrical conductivity. After re-filling the water tank of the test bench, a conductivity of less than 2 µS/cm could be measured for all samples. At later stages of the test campaigns an increase of the electrical conductivity could be observed. However, this had no immediate effect on the performance as the electrolyser has only accumulated a total runtime of a few days.

6.2 Transient behaviour after set point changes

During all tests, it could be observed that the electrolyser exhibits a transient behaviour when the applied voltage is increased or decreased. After a change of the setpoint the electrolyser is not instantaneously operating at a steady operation point again. Instead, the initially achieved current density is shifting and subsequently converging towards a limit value, which is dependent on the given set point. As the current density is decreasing the voltage drop between power supply and electrolyser is also reduced, leading to a raising voltage directly at the electrolyser (U_{WFB}). This effect becomes especially prominent for higher voltages and can be traced back to the relatively long power cables from the power supply to the electrolyser (roughly 10 m). The cable is therefore possessing a non-negligible electrical resistance. Based on ohms-law, this resistance is causing a higher voltage drop for higher currents then for lower ones. Therefore, a decreasing current leads to an increasing voltage at the electrolyser itself, since the setpoint at the power supply is kept constant.

In the left graphs of figure 10, this behaviour is shown exemplary for the first test run at 60 °C during test campaign 1. As can be seen, this behaviour is becoming more prominent towards higher current densities. It has to be noted that the acquired voltage signal has been filtered using a moving-average filter as the voltage measurements exhibited a noticeable noise, possibly caused by the long measurement cables. The resulting signal generated by the moving-average filter has also been compared with the result of a low-pass filter and no noticeable difference of the

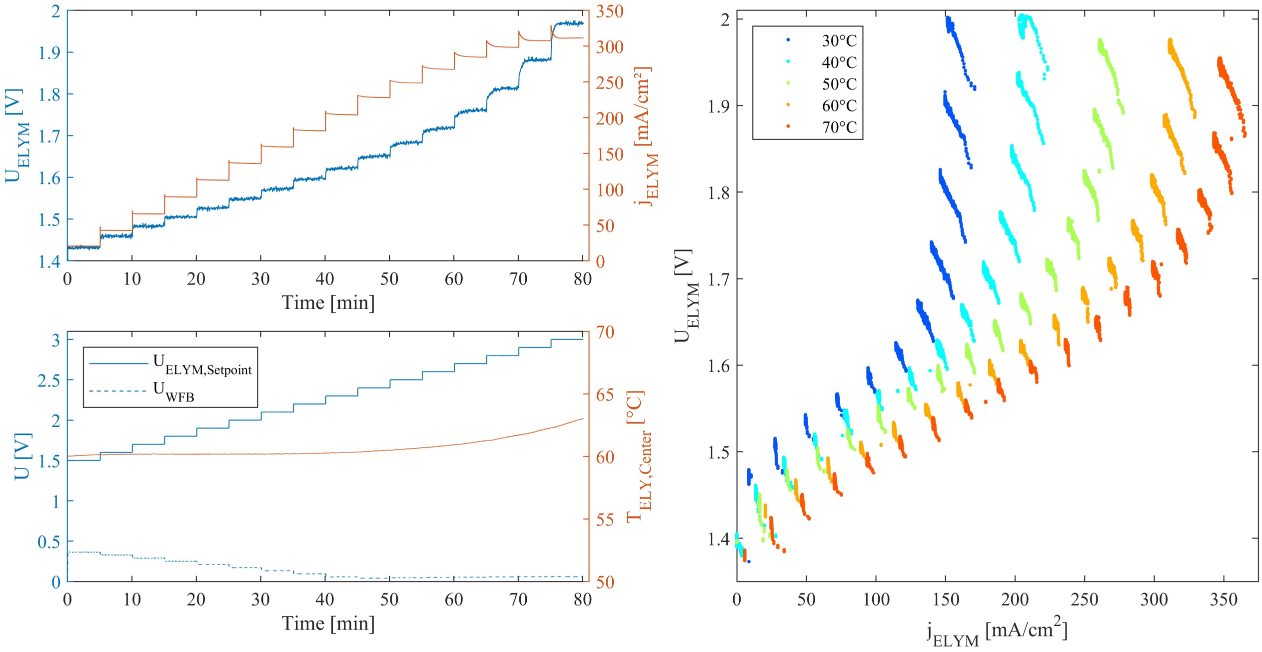

Figure 10: Left side: Evolution of voltage and current density over time at the first test run at 60 °C and atmospheric pressure.
Right side: All collected voltage and current density data points obtained during test campaign 1.

processed signal could be observed. However, as all measurements have been acquired with a rather low frequency of 5 Hz, no underlying voltage fluctuations caused by the electrolyser at specific frequencies could be detected. Potential voltage fluctuations caused by the electrolyser will have to be investigated in future experiments. The applied filter is averaging the acquired voltage values over 3 s, which has been considered sufficiently low in comparison to the holding periods of 5 min per set point.

On the right side of figure 10, all acquired data points of the voltage and current density for each of the different test runs during test campaign 1 are shown in a voltage-current density chart. Each dot represents one measured data point, while each point cloud is showing a specific setpoint. By comparison with the left graphs, it becomes obvious that for each new setpoint the data points start on the right side of the point cloud and are then converging towards their limit on the left side. This behaviour can therefore also be a valid explanation why the polarisation curves in previous publications ([5] and [8]) showed that the current density started to decrease again when a certain voltage has been exceeded (see Figure 15). The cause could be, that set point has not been maintained for a sufficient time until the parameters could settle towards their limit value and instead a higher value has been recorded for some setpoints, leading to a seemingly reversing curve.

In order to obtain the polarization curves for a steady operation of the electrolyser each setpoint was therefore maintained for 5 min, while only the measured parameters during the last 30 seconds were used to acquire their mean values. This method was applied to all following data that is presented.

6.3 Collapse of current density at high temperatures

However, a new phenomenon could be observed that has not been published before in the context of Cathode-Vapour-Feed electrolysers. Figure 11 shows the evolution of the current density and voltage of a test run at 80 °C during test campaign 1. As can be seen, the electrolyser shows the same behaviour as for lower temperatures at first. However, during the last setpoint the current density starts to decrease and is not stabilizing anymore, causing a continuously stepper drop. As described above, the increasing voltage at the constant setpoint is caused by the decreasing voltage drop in the power cables. Once a voltage of 2V is reached the Over-Voltage-Protection of the test bench engages and is reducing the setpoint, to avoid damaging the electrolyser. Although the setpoint is decreased, the current density is dropping far below the values at which the electrolyser could be steadily operated before and is not showing any signs of convergence. Only a complete shutdown and re-start has enabled a further operation of the electrolyser. However, the event seemed to have no damaging impact on the electrolyser, as normal operation could be re-established at lower temperatures afterwards. During a subsequent disassembly of the electrolyser also no damages to any components, e.g.

DOI: 10.13009/EUCASS2023-438

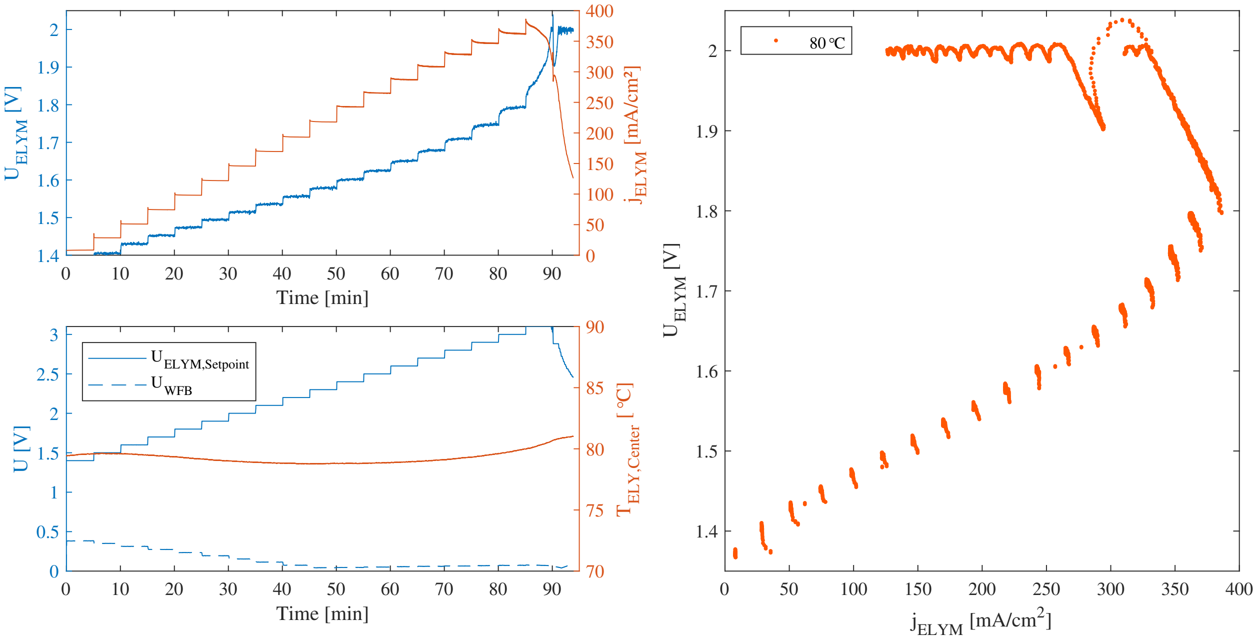

Figure 11: Collapse of current density j at 80 °C and atmospheric pressure

the membranes, were found. The behavior has been reproducible and could also be observed at a temperature of 75 °C. For the maturation towards flight readiness it is therefore crucial to thoroughly understand this phenomenon.

6.4 Electrolyser Performance

Figure 12 shows the polarization curves at different temperatures that were obtained during the 3 test campaigns. During test campaign 1 the highest performance of the electrolyser could be observed. While it showed a significant performance decrease of up to 46 mA/cm^2 during test campaign 2. The most probable cause for the degradation was a potential delamination of the catalyst layers on the CCM as well as damages to the GDLs and their microporous layers (MPL), that have been caused by the disassembly and re-assembly of the electrolyser. As described above it was therefore decided to replace the re-used membranes and GDLs with new ones, in an attempt to restore the initial performance. The renewal of these components had indeed a noticeable and positive impact on the achievable current densities at all temperatures. During test campaign 3, the polarization curves at 50 °C, 60 °C and 70 °C were

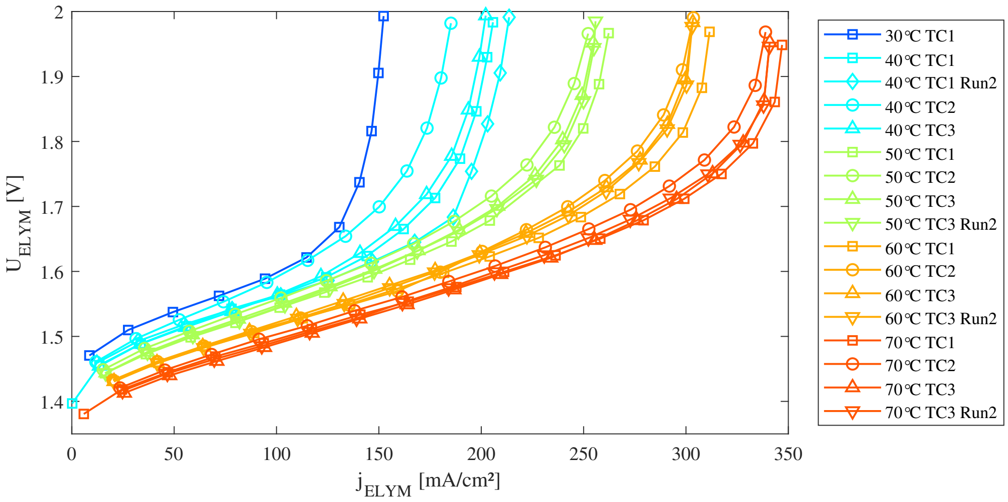

Figure 12: Measured polarisation curves at different temperatures acquired during the test campaigns at atmospheric pressure

DOI: 10.13009/EUCASS2023-438

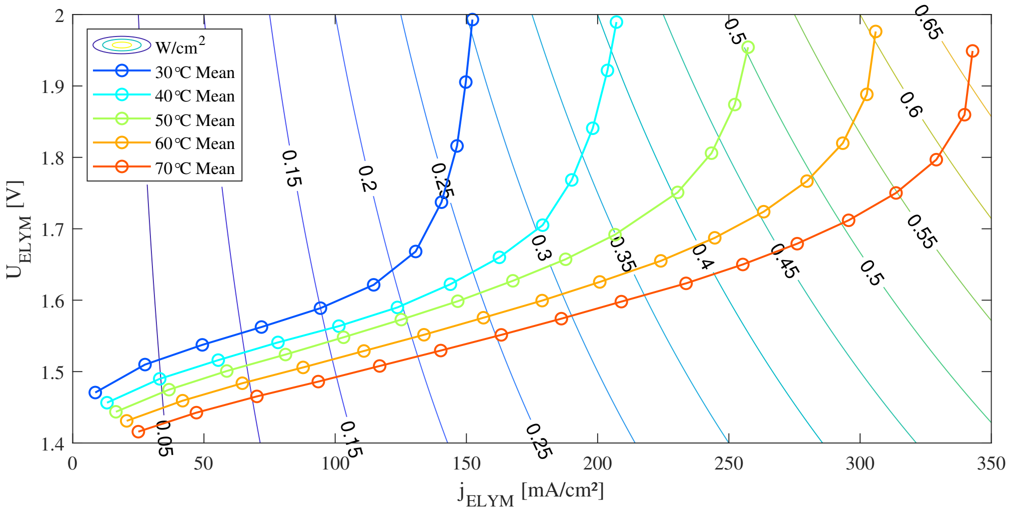

Figure 13: Mean polarisation curves of the investigated electrolyser at different temperatures

conducted twice. As can be seen in Figure 12, the resulting polarization curves are almost identical, showing a good reproducibility of the measurements.

In order to obtain widely useable reference values, the measured polarization curves were used to determine the mean performance of the electrolyser (see Figure 13). For this purpose, only test campaign 1 and 3 were used, as these were not containing any known damages to the membranes or any other essential components of the electrolyser. The derived polarization curves can subsequently be used as a reference for future experimental and theoretical studies on Cathode-Vapour-Feed electrolysers and the WEP technology as a whole. The acquired values are therefore also stated in table 4 for simple re-use.

The obtained reference values have subsequently been used to determine the various efficiencies of the electrolyser. The voltage efficiency can be calculated directly based on the measured voltage values (U_{op}). Based on the higher

Table 4: Mean voltage and current values of the investigated electrolyser at different temperatures

30 °C		40 °C		50 °C		60 °C		70 °C	
U [V]	**j [mA/cm^2]**	**U [V]**	**j [mA/cm^2]**	**U [V]**	**j [mA/cm^2]**	**U [V]**	**j [mA/cm^2]**	**U [V]**	**j [mA/cm^2]**
1.993	152.3	1.989	207.2	1.954	257.3	1.976	305.9	1.949	342.9
1.905	149.8	1.922	203.8	1.874	252.3	1.888	302.6	1.86	339.8
1.816	146.4	1.841	198.1	1.806	243.4	1.82	293.4	1.797	329.0
1.737	140.5	1.768	190.1	1.751	230.5	1.767	279.8	1.75	313.7
1.668	130.7	1.705	179.0	1.692	206.6	1.724	263.3	1.712	295.6
1.621	114.7	1.66	162.6	1.657	187.8	1.687	244.6	1.679	276.0
1.589	94.4	1.622	143.9	1.627	167.7	1.655	224.1	1.65	255.3
1.562	71.9	1.59	123.7	1.599	146.7	1.626	200.8	1.624	233.7
1.537	49.4	1.564	101.4	1.573	125.2	1.599	178.9	1.598	209.0
1.51	27.6	1.541	78.2	1.548	103.2	1.575	156.5	1.574	186.2
1.471	8.6	1.516	55.5	1.524	81.1	1.552	133.8	1.551	163.3
		1.49	33.2	1.501	58.7	1.529	111.0	1.529	140.2
		1.456	13.1	1.475	36.7	1.506	87.8	1.508	117.0
				1.444	16.5	1.484	64.6	1.486	93.6
						1.459	41.9	1.465	70.2
						1.431	20.6	1.443	47.1
								1.416	25.0

DOI: 10.13009/EUCASS2023-438

Table 5: "Numeric values of the parameters used for the model" [13]

Gas	**A**	$\epsilon^{\mathbf{diff}}$	$\epsilon^{\mathbf{dp}}$
H_2	$2.4\,\mathrm{bar\,cm^2/A}$	$4.65\times10^{-11}\,\mathrm{mol/(cm\,s\,bar)}$	$2\times10^{-11}\,\mathrm{mol/(cm\,s\,bar)}$
O_2	$2.8\,\mathrm{bar\,cm^2/A}$	$2\times10^{-11}\,\mathrm{mol/(cm\,s\,bar)}$	–

heating value (HHV) of water, it can be determined using equation 6 and 9 [12].

$$\eta_U = \frac{U^0_{th}}{U_{ELY}} \tag{9}$$

As commonly known the faradaic efficiency is defined by equation 10 and therefore dependant on the molar flow of the generated hydrogen ($\dot{n}_{H_2,op}$) [4].

$$\eta_I = \frac{\dot{n}_{H_2,op}}{\dot{n}_{H_2,theor}} = \frac{\dot{n}_{H_2,op}}{I(z_{\mathrm{H_2}}F)^{-1}} \tag{10}$$

As $\dot{n}_{H_2,op}$ cannot be measured directly, it has to be determined by a measurement of the mass flow combined with a measurement of the hydrogen concentration at the cathodic outlet of the electrolyser. However, at the time of conducting the test campaigns such measurements could not successfully be performed for all test runs. In order to make a qualitative assessment of the achieved cell efficiency nevertheless, the faradaic efficiency is calculated using the method presented by Schalenbach et al [13]. The method is using the gas permeation flux densities $\Phi^{en}_{\mathrm{H_2}}$ and $\Phi^{en}_{\mathrm{O_2}}$ as well as the gas production rate densities $\Gamma_{\mathrm{H_2}}$ and $\Gamma_{\mathrm{H_2}}$ to calculate the faradaic efficiency. At first the partial pressures of hydrogen in the cathode catalyst layer $p^{cat}_{\mathrm{H_2}}$ and of oxygen in the anode catalyst layer $p^{an}_{\mathrm{O_2}}$ is determined using equation 12 and 11, while utilizing the empirical parameters stated in table 5. The parameters p^{cat} and p^{an} denote the total pressure at the cathodic outlet and anodic outlet, respectively. As all tests have been conducted at atmospheric pressure, they are assumed to be equal to 1 bar.

$$p^{an}_{\mathrm{O_2}} = p^{an} + A_{\mathrm{O_2}} j \tag{11}$$

$$\begin{aligned} p^{cat}_{\mathrm{H_2}} =& [p^{cat}\epsilon^{dif}_{\mathrm{H_2}} \pm (p^{cat2}\epsilon^{dif^2}_{\mathrm{H_2}} + 2p^{cat}A_{\mathrm{H_2}}\epsilon^{dif^2}_{\mathrm{H_2}} j + 2p^{cat}A_{\mathrm{H_2}}\epsilon^{dif}_{\mathrm{H_2}}\epsilon^{dp}_{\mathrm{H_2}} j \\ &+ A^2_{\mathrm{H_2}}\epsilon^{dif^2}_{\mathrm{H_2}} j^2 + 2A^2_{\mathrm{H_2}}\epsilon^{dif}_{\mathrm{H_2}}\epsilon^{dp}_{\mathrm{H_2}} j^2 + A^2_{\mathrm{H_2}}\epsilon^{dp^2}_{\mathrm{H_2}} j^2 - 4p^{an}_{\mathrm{O_2}}A_{\mathrm{H_2}}\epsilon^{dif}_{\mathrm{H_2}}\epsilon^{dp}_{\mathrm{H_2}} j)^{\frac{1}{2}} \\ &+ A_{\mathrm{H_2}}\epsilon^{dif}_{\mathrm{H_2}} j + A_{\mathrm{H_2}}\epsilon^{dp}_{\mathrm{H_2}} j]/(2\epsilon^{dif}_{\mathrm{H_2}}) \end{aligned} \tag{12}$$

Subsequently, the gas permeation flux densities of both gases $\Phi^{en}_{\mathrm{H_2}}$ and $\Phi^{en}_{\mathrm{O_2}}$ can be calculated utilizing equations 13 and 14. Parameter d describes the membrane thickness. In order to consider the swelling of the membrane caused by its hydration during the operation of the electrolyser the thickness of $d = 127\,\mu\mathrm{m}$ of the used Nafion© 115 membranes was increased by 14% for the calculation, as suggested by Schalenbach et al [13].

$$\Phi^{en}_{\mathrm{O_2}} = \epsilon^{diff}_{\mathrm{O_2}} \frac{p^{an}_{\mathrm{O_2}}}{d} \tag{13}$$

$$\Phi^{en}_{\mathrm{H_2}} = \epsilon^{diff}_{\mathrm{H_2}} \frac{p^{cat}_{\mathrm{H_2}}}{d} + \epsilon^{dp}_{\mathrm{H_2}} \frac{p^{cat}_{\mathrm{H_2}} - p^{an}_{\mathrm{O_2}}}{d} \tag{14}$$

Afterwards, the gas production rate densities of the hydrogen $\Gamma_{\mathrm{H_2}}$ and the oxygen $\Gamma_{\mathrm{H_2}}$ can be calculated [13].

$$\Gamma_{\mathrm{H_2}} = \frac{j}{2F} \qquad \text{in mol/cm}^2\text{s} \tag{15}$$

$$\Gamma_{\mathrm{O_2}} = \frac{j}{4F} = \frac{1}{2}\Gamma_{\mathrm{H_2}} \qquad \text{in mol/cm}^2\text{s} \tag{16}$$

Now the faradaic efficiency can be obtained by equation 17 as well as the mass fraction of hydrogen in oxygen by equation 18 [13].

$$\eta_F = 1 - \frac{\Phi^{en}_{\mathrm{H_2}}}{\Gamma_{\mathrm{H_2}}} - 2\frac{\Phi^{en}_{\mathrm{O_2}}}{\Gamma_{\mathrm{H_2}}} \tag{17}$$

$$\mathrm{H_2 \text{ in } O_2} = \frac{\Phi^{en}_{\mathrm{H_2}}}{\Gamma_{\mathrm{O_2}} + \Phi^{en}_{\mathrm{H_2}}} \times 100\% \tag{18}$$

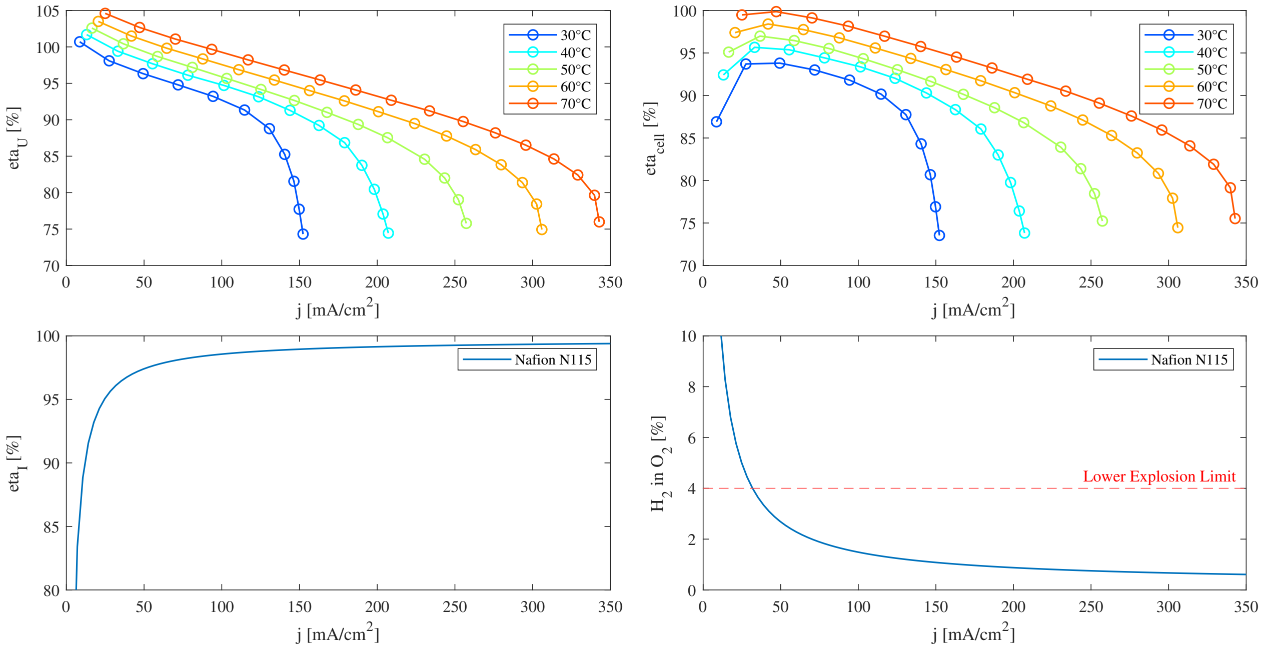

Figure 14: Top left: Voltage efficiency η_U based on the HHV and the measured voltages.
Top right: theoretical cell efficiency η_{cell}. Bottom left: theoretical faradaic efficiency η_I.
Bottom right: theoretical H_2 content in O_2 at the anodic outlet

The resulting voltage, faradaic and cell efficiencies as well as the expected permeation of H_2 into O_2 at the anodic outlet based on the mean polarisation curves of the electrolyser are depicted in figure 14. As can be seen in the top left graph, the voltage efficiency is exceeding an efficiency of 100%. The reason for this behavior is that some of energy required for the reaction is consumed as heat from the surrounding, effectively cooling the electrolyser. Obviously the overall cell efficiency can not be higher than 100%. Moreover, it has to be noted that the shown graphs for η_I and η_{cell} might under or overpredict the actual efficiencies. However, they can already provide a qualitative impression of the their behavior. Further investigation to determine the faradaic efficiency and thus the cell efficiency by measurement are crucial for the further development of the Cathode-Vapour-Feed technology.

7. Comparison

As previously mentioned, there are only very few publications in which the performance of modern CVF electrolysers are discussed. Nevertheless, the obtained measurements shall be compared with the available data. Figure 15 shows the polarization curves of a proof of concept CVF electrolyser published in [5] and [8] in which this particular electrolyser is referred to as 'Lab Model'. The flow field of this electrolyser follows a different design approach then the presented one, as it only consists of various holes drilled through the monopolar plate, resulting in a porosity of 48.39%. In addition, the thickness of the H_2-monopolar plate is 9.8 mm, causing a relatively large distance between the electrolysis membrane (ELYM) and the Water-Feed-Barrier (WFB).

It can be observed that for this 'Lab Model' the current is starting to flow at higher voltages in comparison to the presented electrolyser (see figure 13). However, it is unclear whether the voltage of the 'Lab Model' has been measured directly at the electrolyser or at the power supply. A voltage measurement at the power supply would result in an additional resistance caused by the power cables to and from the electrolyser and therefore an increased voltage reading. Nevertheless, the presented electrolyser achieves significantly higher maximum current densities. The 'Lab Model' reaches 194 mA/cm^2 at ~2 V and 70 °C while the presented electrolyser reaches 343 mA/cm^2 at ~1.95 V at the same temperature, resulting in a performance increase of ~77%. In addition, the slope of the polarisation curve during the rather linear section can be used to approximate the ohmic resistance of the electrolyser. This results in an ohmic resistance of 1.5 to 2 Ω/cm^2 for the 'Lab Model', while for the presented electrolyser an ohmic resistance of ~0.9 Ω/cm^2 could be determined. Moreover, a possible cause for the reversing polarisation curve of the 'Lab Model' at higher voltages could be identified in the previous sections.

Figure 16 shows the latest published polarisation curves of the CVF electrolyser currently in development at ArianeGroup GmbH [14] [15]. There are no detailed information about its design publicly available, but images show

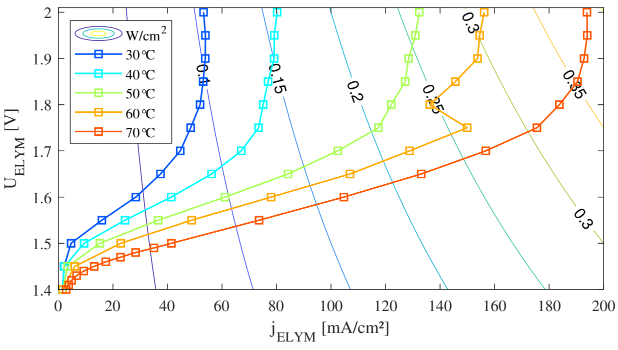

Figure 15: Polarisation curves of a proof of concept CVF electrolyser published by [5] and [8]

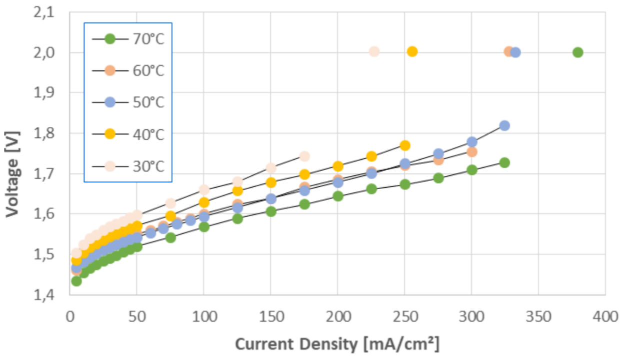

Figure 16: Polarisation curves of a CVF electrolyser of ArianeGroup GmbH [14]

that the H_2-monopolar plate is quite thin and therefore the distance of the membranes is small as well. Similar as in the 'Lab Model' of [5] and [8], the current is starting to flow at higher voltages than in the presented electrolyser, potentially due to the same reason. It achieves a current density of $380\,\mathrm{mA/cm^2}$ at ~2 V and 70 °C and its ohmic resistance can be approximated as $\sim 0.7\,\Omega/\mathrm{cm}^2$. In conjunction with the presented results in the previous sections it becomes obvious that the distance between the two membranes might have a significant impact and has to be investigated further.

In summary, it can be said that the presented electrolyser is reaching ~90% of the performance of the currently leading CVF-electrolyser from the European industry. The similar performance is therefore enabling a use of the presented measurement data to serve as a reference for future developments and improvements in the field of Cathode-Vapour-Feed electrolysers for space applications.

8. Conclusion and Outlook

The investigated electrolyser achieved current densities of more than $300\,\mathrm{mA/cm^2}$ in testing. In general, the electrolyser shows a similar performance as published for state-of-the-art Cathode-Vapour-Feed (CVF) electrolysers and can therefore be used when conducting theoretical studies on the topic of Water Electrolysis Propulsion.

It could be observed that the distance between the electrolysis membrane (ELYM) and the Water-Feed-Barrier (WFB) plays an important role in achieving high current densities. However, the investigation also revealed the electrolyser's unstable behaviour at high current densities and temperatures above 70 °C, exhibiting a complete collapse of the current density from which it could only recover after a complete restart. The origin of this behaviour will have to be investigated in more detail as it could damage the system during flight operations.

The voltage efficiency could be determined based on the measured values and the faradaic and resulting cell efficiency could be shown qualitatively using a theoretical model. A fully experimental determination of all efficiencies as well as the cross-diffusion and humidity content of the produced gases remains to be crucial for the maturation of the technology. This is also the case for the impact of the water quality on the longevity of the electrolyser as well as its performance at increased pressures.

The maturation of the electrolyser design towards flight readiness will continue at the Technical University of Munich (TUM), where a new prototype and test bench is currently in preparation. However, the presented data can support upcoming system and mission analyses for spacecraft missions aiming to use Water Electrolysis Propulsion and have the potential to serve as reference data for future research in the area [16]. Furthermore, the presented electrolyser has already successfully been used to provide gases for a Hall Effect Thruster in a coupled operation. A respective publication will follow [10].

Acknowledgments

The corresponding author designed the presented electrolyser, the mentioned test bench and conducted the various test campaigns during his time as German Trainee at the European Space Research and Technology Centre (ESTEC) of the European Space Agency (ESA). He wishes to thank the German Aerospace Center (DLR) for the granted scholarship within the German Trainee Programme, which enabled the stay at ESA and therefore also the presented work.

DOI: 10.13009/EUCASS2023-438

References

[1] Euroconsult, "Satellites to be Built & Launched by 2030," Tech. Rep., Dec. 2021.

[2] A. Herbertz, N. Arcis, D. Feili, N. Fernandes, J. F. Alsina, A. Garbayo, U. Gotzig, S. Heizmann, S. Hyde, A. Knoll, J. Sadler, D. Staab, F. V. Bel, J. Vilag, and S. Wilson, "Overview of Water Electrolysis Propulsion Research at ESA," in *8th Edition of the Space Propulsion Conference*, Estoril, Portugal, 2022.

[3] A. Herbertz, "Theoretical Performance and Application Cases of Water Electrolysis Propulsion," *Transactions of the Japan Society for Aeronautical and Space Sciences, Aerospace Technology Japan*, vol. 19, no. 2, pp. 199–204, 2021.

[4] D. Bessarabov, H. Wang, H. Li, and N. Zhao, *PEM Electrolysis for Hydrogen Production Principles and Applications*. CRC Press, Jul. 2017.

[5] S. Heizmann, "Development of a Miniaturized PEM Electrolyzer for a Small Satellite Application," Master's thesis, University of Stuttgart, Stuttgart, Germany, 2018.

[6] Q. Yan, H. Toghiani, and J. Wu, "Investigation of water transport through membrane in a PEM fuel cell by water balance experiments," *Journal of Power Sources*, vol. 158, no. 1, pp. 316–325, Jul. 2006.

[7] Y. Sone, P. Ekdunge, and D. Simonsson, "Proton Conductivity of Nafion 117 as Measured by a Four-Electrode AC Impedance Method," *Journal of The Electrochemical Society*, vol. 143, no. 4, pp. 1254–1259, Apr. 1996.

[8] N. Harmansa, "Entwicklung und Charakterisierung eines Satellitenantriebssystems basierend auf Wasserelektrolyse," Ph.D. dissertation, University of Stuttgart, 2020.

[9] J. Saryczew, S. Heizmann, and A. Herbertz, "Development of a Test Bench for Electrolyser Performance Evaluation for Water Electrolysis Propulsion," in *34th International Symposium on Space Technology and Science*, Kurume, Japan, 2023.

[10] J. Tejeda, M., J. Saryczew, and et al., "First end-to-end experimental demonstration of a water electrolysis Hall Effect Thruster," *IAA ACTA Astronautica, (to be published).*

[11] "Freudenberg Gas Diffusion Layers," https://fuelcellcomponents.freudenberg-pm.com/-/media/Files/fuelcellcomponents,-d-,freudenbergpm,-d-,com/FPM_technical-data-sheet_electrolysis_ENG_2022-02-11.pdf, Jun. 2023.

[12] K. W. Harrison, R. Remick, G. D. Martin, and A. Hoskin, "Hydrogen Production: Fundamentals and Case Study Summaries; Preprint," in *18th World Hydrogen Energy Conference*, ser. NREL/CP-550-47302, Essen, Germany, May 2010.

[13] M. Schalenbach, M. Carmo, D. L. Fritz, J. Mergel, and D. Stolten, "Pressurized PEM water electrolysis: Efficiency and gas crossover," *International Journal of Hydrogen Energy*, vol. 38, no. 35, pp. 14 921–14 933, Nov. 2013.

[14] N. Harmansa, M. Wurdak, and U. Gotzig, "Latest Developments of the Water Propulsion System Electrolyzer," in *SPACE PROPULSION 2022*, ser. SP2022_255, ESTORIL, PORTUGAL, May 2022.

[15] U. Gotzig, M. Wurdak, and N. Harmansa, "Development and coupled thruster / electrolyser tests of a water propulsion system," *Acta Astronautica*, vol. 202, pp. 751–759, Jan. 2023.

[16] S. Dengler, A. Wagmann Y Otero, and C. Manfletti, "Optimising ConOps of Water Electrolysis Propulsion systems using Deep Q-Learning: A Proof-of-Concept," in *Aerospace Europe Conference 2023 - 10th EUCASS - 9th CEAS*, Lausanne, Switzerland, Jul. 2023.